High performance $La_2NiO_{4+\delta}$-infiltrated $(La_{0.6}Sr_{0.4})_{0.995}Co_{0.2}Fe_{0.8}O_{3-\delta}$ cathode for solid oxide fuel cells

CrossMark

Xinxin Zhang, Hui Zhang, Xingbo Liu*

Mechanical & Aerospace Engineering Department, Benjamin M. Statler College of Engineering & Mineral Resources, West Virginia University, P.O. Box 6106, Morgantown, WV 26506-6106, USA

HIGHLIGHTS

- LNO was infiltrated to LSCF as SOFC cathode.
- Peak power density of SOFC with LSCF cathode increased by 67% via LNO infiltration.
- The infiltrated cathode shows similar stability as the LSCF baseline.

ARTICLE INFO

ABSTRACT

In this paper, we reported our effort on improving electrochemical performance of $(La_{0.6}Sr_{0.4})_{0.995}Co_{0.2}Fe_{0.8}O_{3-\delta}$ (LSCF) cathode in solid oxide fuel cell (SOFC) by infiltration of $La_2NiO_{4+\delta}$ (LNO). It is found that a porous LSCF backbone coated with LNO nanoparticles is an attractive way to acquire a noticeable decrease in the polarization resistance and activation energy of LSCF cathode, thereby showing high surface activity and enhanced oxygen transport capability. The key contributions of the LNO nanoparticles also lead to a 67% increase in peak power density and operation stability at a constant current density of 250 mA cm^{-2} with a low degradation rate of 0.39% for about 500 h at 750 °C. Although extended durability of LNO-infiltrated LSCF might be concerned, based on coarsening of the LNO nanoparticles, a greatly increased power density and voltage output after a cell operation of 500 h engenders substantial confidence in the beneficial effect of LNO-infiltrated LSCF materials on cell properties. The enhancement of ORR kinetics could be ascribed to the increase of active surface area and active reaction regions from the heterostructured LSCF/LNO interface architecture, and/or favorable cation diffusion from LSCF to LNO.

© 2014 Elsevier B.V. All rights reserved.

1. Introduction

Although a great deal of research has been conducting to develop new cathode materials [1–4], for operation at lower temperatures (500–750 °C), $La_{1-x}Sr_xCo_{1-y}Fe_yO_{3-\delta}$ (LSCF) based cathodes are by far the most popularly used for solid oxide fuel cells (SOFCs) today. The iron and cobalt-containing LSCF perovskite materials have high ionic and electronic conductivity (about 1×10^{-2} and 10^2 S cm^{-1} at 800 °C [5]), respectively, leading to the extension of the electrochemically active region to a finite width from the electrode/electrolyte interface. However, the main challenges associated with long-term application of LSCF based

cathodes are material instability such as Sr segregation and surface-limiting oxygen reduction reaction (ORR) process [6–8]. Based on a large characteristic length *lc* value, e.g. $lc \approx 0.5$ mm in our previous study [9], the oxygen transport in LSCF cathode is obviously shown to be surface-limited for oxygen exchange at the gas–cathode interface. Moreover, the Sr segregation in LSCF cathode changes the composition stoichiometry and forms inactive surface species (e.g. SrO), which has been considered as a key issue towards inferior catalytic activity for surface ORR kinetics [7]. Hence, the surface exchange capability of LSCF based cathodes would be further inhibited, giving rise to polarization loss and cell degradation.

To alleviate the problems of LSCF based cathodes, high oxygen ion conducting phases like Gd doped ceria (GDC) or noble catalysts like Pd have been introduced into LSCF cathodes. In particular, infiltration has been widely used to fabricate the LSCF based

* Corresponding author. Tel.: +1 304 293 3339; fax: +1 304 293 6689.
  E-mail address: xingbo.liu@mail.wvu.edu (X. Liu).

composite materials. Through the beneficial effect of nano-scale infiltrated particles, the electrocatalytic properties and ORR behavior of LSCF based cathodes can be improved. For example, Chen et al. [10] indicated that GDC infiltration reduced the polarization resistance of LSCF cathode to 0.06 Ω cm^2 compared with 0.22 Ω cm^2 for pure LSCF cathode at 750 °C, Liu et al. [11] demonstrated that the polarization resistance for SDC-infiltrated LSCF cathode was lowered to half of that for LSCF cathodes without infiltration of SDC. Kilner et al. [12] reported that the electrocatalytic performance of an LSCF cathode can be enhanced by the infiltration of Pd nanoparticles in the temperature range of 400–750 °C.

In this paper, we developed a new LSCF based composite materials prepared by infiltration, namely La$_2$NiO$_{4+\delta}$ (LNO)-infiltrated LSCF. The special interest associated with the employment of LNO materials mainly lies in the sequent three points: 1) Rapid bulk oxygen diffusion and surface oxygen exchange can be offered in the LNO nickelates based on their additional conduction pathway in high concentration of oxygen interstitials. Skinner et al. [13,14] have confirmed that LNO-based materials show a higher bulk oxygen diffusion coefficient D of about 5×10^{-8} cm^2 s^{-1} than that of LSCF materials by one order of magnitude, and a slightly higher surface oxygen exchange coefficient k of about $2-5 \times 10^{-7}$ cm s^{-1} at 700–750 °C. 2) LNO as a Sr acceptor seems extremely promising to improve cathode stability and electrocatalytic properties without invoking deleterious LSCF surface reactions related to the formation of inactive Sr species. Reports [13,15,16] have shown there is an obvious increase in the electronic conductivity and oxygen transfer capability of Sr-containing LNO in comparison to LNO itself. Unlike previous researches [17–20] attempting to physically suppress Sr-enrichment on the surface of LSCF by the application of surface thin films, a chemical driving force in the LNO/LSCF combination is expected for diffusion of Sr from LSCF into LNO to benefit surface oxygen exchange and material stability of the composite cathode. 3) A heterostructured interface would potentially extend the active regions of two phase boundary (2PB, LSCF/LNO) and triple phase boundary (TPB, LSCF/LNO/gas) with high oxygen transfer capability, leading to total ORR kinetic enhancement of the SOFC cathode. Efforts in the development of (La,Sr)CoO$_{3-\delta}$/(La,Sr)$_2$CoO$_{4+\delta}$ (LSC113/LSC214) heterostructured architecture via pulsed laser deposition (PLD) have been made by Crumlin et al. [21,22]. It was found that interfacial regions are responsible for enhanced ORR kinetics of ~3 orders of magnitude for the entire electrode with surface decorations of LSC214 relative to bulk LSC 113. For these reasons, the main aim of this study is to examine the influence of LNO infiltrated into porous LSCF cathode, from both a scientific and technological point of view, on ORR behavior and long-term stability of the LNO-infiltrated LSCF cathodes.

2. Experimental process

The effect of LNO infiltration on the electrochemical properties of LSCF cathodes was first investigated by the use of electrochemical impedance characterizations of symmetric cells. A symmetric cell configuration of LSCF|GDC|YSZ|GDC|LSCF was assembled starting with the preparation of 8% Y$_2$O$_3$-stabilized ZrO$_2$ (YSZ, TZ8Y, Tosoh, Japan) electrolyte supports. A tape casting technique followed by sintering at 1450 °C for 5 h was used to form dense YSZ electrolyte pellets with a thickness of about 300 μm. Then, identical GDC buffer layers were screen printed symmetrically on both sides of the YSZ electrolyte and then sintered at 1200 °C, in order to avoid interaction between YSZ electrolyte and LSCF cathode. A-site deficient (La$_{0.6}$Sr$_{0.4}$)$_{0.995}$Co$_{0.2}$Fe$_{0.8}$O$_{3-\delta}$ (LSCF) powder, which was received from Fuel Cell Material Co. in US., was dispersed into an organic vehicle ink (VHE, Fuel Cell Material Co. in US.) to form a slurry. By a subsequent screen printing process, porous LSCF layers with a thickness of 10–20 μm were applied onto the GDC buffer layers. Eventually, the bonded layers were co-fired at 1150 °C for 3 h to obtain a symmetric cell with an active surface area of about 0.7 cm^2. For comparison and performance evaluation, LNO was infiltrated into both sides of the LSCF layers in the LSCF|GDC|YSZ|GDC|LSCF cell, as described below, to form a symmetric cell using LNO infiltrated LSCF cathode.

The LNO precursor solution with a concentration of 1 mol L^{-1} was composed of La(NO$_3$)$_3$·6H$_2$O and Ni(NO$_3$)$_2$·6H$_2$O (99.9%, Alfa Aesar) dissolved in mixture of ethanol and deionized water with a ratio of 1:0.6. We confirmed that an appropriate amount of ethanol can promote the formation of LNO phase and improve its distribution status on the LSCF substrate. The infiltration solution was then dropped slowly into both sides of the porous LSCF substrate using milliliter syringe. Each infiltration step was followed by pre-sintering to 250 °C in air to dry the samples. Repeated infiltration followed by the drying process was carried out to increase the amount of LNO phase in the modified cathode. After 5 times repeating, the cells were sintered at 900 °C for 1 h to allow the formation of LNO single phase with 15.9 wt% loading on the LSCF backbone.

Prior to electrochemical characterization, Pt meshes were attached as current collectors to both electrode sides of the symmetric cells by using Pt paste. The electrochemical impedance spectroscopy (EIS) measurements for the symmetrical cells were carried out by a Metrohm Autolab test station (AUT85484) in ambient air under open circuit voltage (OCV). The frequency range was 0.1–100 kHz at an amplitude of alternating circuit (AC) signal of 10 mV, and the measured temperature was controlled from 550 to 750 °C. A stabilization time of 30 min was utilized before the collection of the impedance data.

For comparison, anode-supported fuel cells using LSCF or LNO infiltrated LSCF cathodes were prepared and measured to form NiO-YSZ|YSZ|GDC|LSCF and NiO-YSZ|YSZ|GDC|LNO-infiltrated LSCF. Anode-supported half fuel cells Ni-YSZ/YSZ were commercially available (MSRI, Salt Lake City, UT), consisting of about 10 μm-thick YSZ electrolyte and 750 μm-thick Ni-YSZ anode. The GDC buffer layer and bare/modified LSCF cathodes were sequentially applied to the YSZ electrolyte using the same procedures for the fabrication of symmetric cells as mentioned above. The whole cells were then sealed using mica materials, attached by using Pt meshes with Pt paste for cathode and Ni paste for anode, and fixed in a conventional single cell test stand (installed at NETL, Morgantown,WV site).

The on cell measurements were eventually performed at 750 °C with dry hydrogen as the fuel for anode and ambient air as the oxidant for cathode with each at a flow rate of 400 sccm. A constant current density of 250 mA cm^{-2} was applied to the fuel cells using a DC electronic load to monitor the long-term stability of SOFC cathodes. In addition to the continuous observations of the changes in cell voltage, the intermittent current–voltage curves were also carried out by using a Solartron 1287 electrochemical interface combined with a Solartron 1260 frequency response analyzer. A Panalytical X'pert Pro X-ray diffractometer (XRD) with Cu Kα radiation (λ = 1.5406 Å) was used to identify phase composition and crystalline structure. The surface morphology analyses for both LSCF and LNO infiltrated LSCF materials were performed using a field emission scanning electronic microscope (FESEM, JEOL 7600F) at an acceleration voltage of 20 kV. Transmission electron microscopy (TEM) observations and elemental identifications were also carried out on a JEOL JEM-2100 LaB$_6$ microscope equipped with an energy dispersion spectrometry (EDAX, Evex NanoAnalysis).
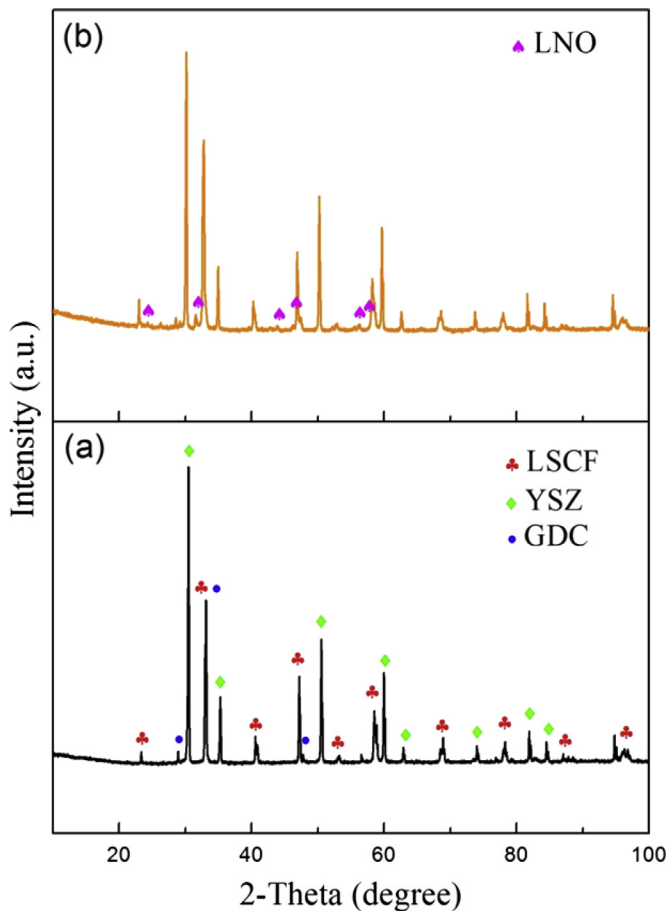
Fig. 1. XRD patterns of (a) bare LSCF cathode and (b) LNO-infiltrated LSCF on GDC/YSZ electrolyte.

3. Results and discussion

3.1. Characterization analysis

Fig. 1 displays the XRD patterns of LSCF pellets with and without LNO infiltration. All of the reflections in the diffractogram of the bare LSCF sample on the electrolyte can be labeled in terms of LSCF, GDC and YSZ phases. The appearance of a single Ruddlesden–Popper (RP) phase for LNO infiltrated LSCF sample confirms the existence of LNO

in the LSCF backbone. The diffraction peaks of the LNO phase can be identified as tetragonal K_2NiF_4 structure of I4/mmm space group (JCPDS card No. 34-0314), which shows excellent agreement with those reported in related literature [23]. The typical SEM images of bare LSCF and LNO infiltrated LSCF pellets are depicted in Fig. 2. Based on the clean surface and barren pores existing in the bare LSCF sample, it is obviously noted that the infiltration process leads to the growth of LNO materials with average particle size of about 50 nm. Of importance to note is that the LNO nanoparticles are distributed not only on the surface but also in the pores of LSCF backbone. In particular, the uniform distribution of LNO into LSCF pore walls would promote the formation of more 3PB active sites for ORR enhancement.

3.2. Electrochemical performance of cathodes

Representative EIS data for symmetric cells using bare LSCF or LNO-infiltrated LSCF cathodes collected at OCV in air at temperature of 700 and 750 °C, respectively, are shown in Fig. 3. Typical equivalent circuits have been used to de-convolute the measured data for the cathodes, as displayed in the insets of Fig. 3 (a) and (b), where R is the ohmic resistance of the YSZ electrolyte, and R_n and Q_n indicate resistance and constant phase element of different electrode processes, respectively. In the case of LSCF cathode, two $R–Q$ elements of semi-circle arcs reflect the electrode polarization. An equivalent capacitance value $C_1 (C_i = (R_i Q_i)^{1/n_i}/R_i)$ in the range of $10^{-3}–10^{-2}$ F cm^{-2} is obtained from high frequency response, which is typically attributed to charge transfer process according to literatures [24,25]. Corresponding to C_2 value of ~10^{-2} F cm^{-2}, an intermediate behavior with a similar surface process (e.g. surface diffusion, adsorption/desorption, dissociation, etc.) between gas diffusion and charge-transfer is observed. For LNO-infiltrated LSCF cathode, an additional contribution at low frequency with C_3 value of $10^0–10^1$ F cm^{-2} has also been used for fitting, which may be assigned to gas diffusion as reported elsewhere [26]. Such an equivalent circuit model can well resolve the impedance plots of the symmetric cells using different cathodes. The actual polarization resistance of SOFC cathode (Rp) can thereby be deduced from electrode area and half sum of Rn values (symmetric cell).

The Rp values for bare LSCF cathode are 1.34 Ω cm^2 at 700 °C and 0.62 Ω cm^2 at 750 °C, respectively, which are higher than those in literatures [27,28] reporting Rp ≈ 0.3–0.6 Ω cm^2 at 700 °C and 0.1–0.3 Ω cm^2 at 750 °C. This could be explained by the relatively higher sintering temperature of 1150 °C applied here for the LSCF cathode, leading to decreased surface area and more Sr segregation. For comparison, LNO-infiltrated LSCF cathode decreases the Rp
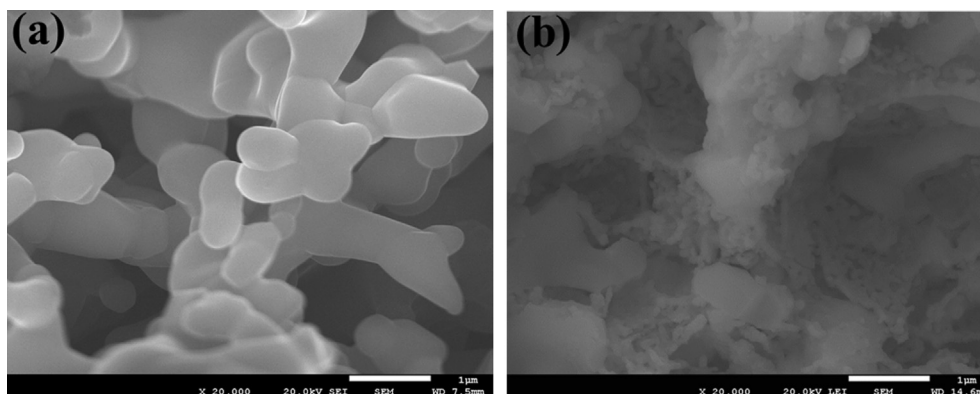

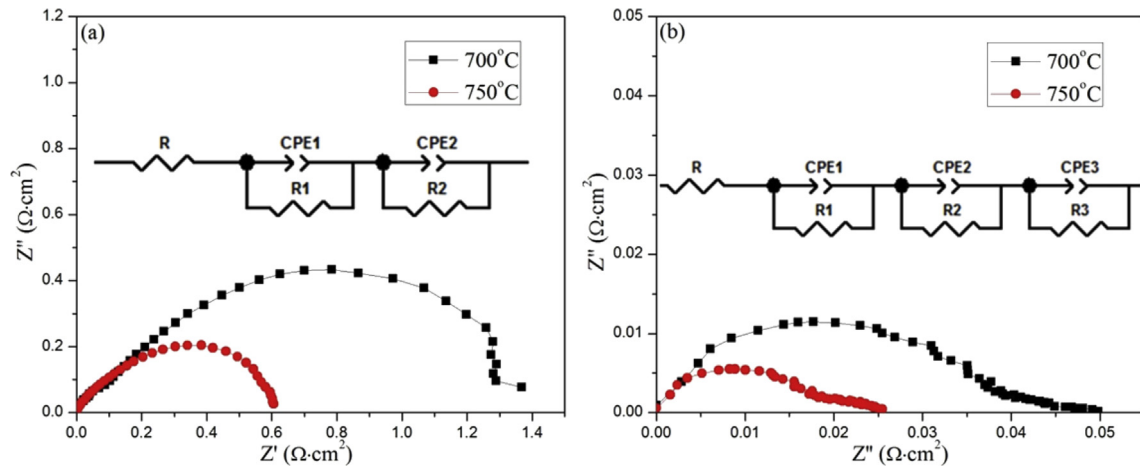**Fig. 2.** SEM images of (a) bare LSCF cathode; and (b) LNO-infiltrated-LSCF materials.

Fig. 3. Typical electrochemical impedance spectra of symmetrical cells using LSCF cathodes (a) without and (b) with LNO infiltration under OCV at 700 and 750 °C.

values to 0.042 Ω cm² at 700 °C and 0.023 Ω cm² at 750 °C. The obvious reduction in cathode polarization resistance demonstrates that LNO infiltration enhances the electrochemical activity and surface exchange kinetics of LSCF electrodes. Additionally, temperature-dependent polarization resistance is also characterized in Fig. 4, and activation energy (Ea) for the electrode polarization contribution can be calculated from the linear relationship of $\ln R_p^{-1}/T$ by using Arrhenius law. It can be observed that the activation energy drops from 1.38 eV to 1.06 eV after the infiltration of LNO into LSCF. Hence, LNO can be further evaluated as an effective catalyst to enhance ORR reaction kinetics and electro-catalytic activity of LSCF cathode. The performance improvement could be the result of nano-scale LNO fine particles increasing the surface active area, heterostructured LSCF/LNO interface architecture offering more active reaction regions of 2PB and 3PB, and/or favorable cation diffusion from LSCF to LNO facilitating oxygen exchange and transport.

3.3. Long-term stability of cathodes

Fig. 5 presents the current−voltage characteristics and the corresponding power density for anode-supported fuel cells using

bare LSCF or LNO-infiltrated LSCF cathodes during long-term operation of about 500 h at 750 °C. The open circuit voltages (OCVs) for both on-cells are very close to the theoretical value derived from the Nernst equation, which demonstrates that the cells were well sealed with a gas-tight electrolyte. The power
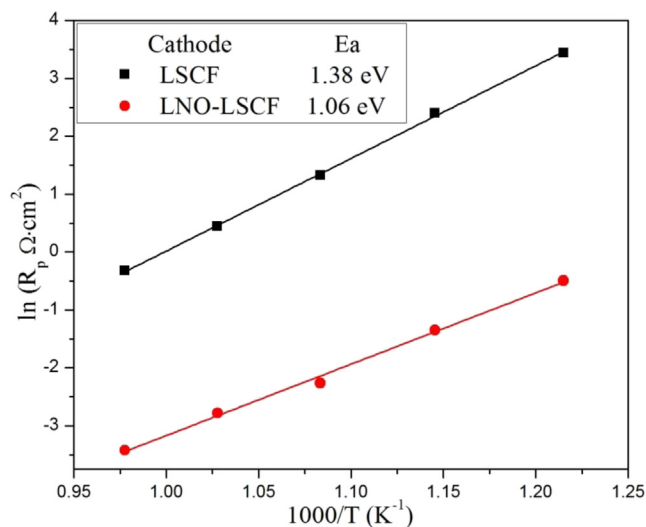

Fig. 4. Cathode polarization resistance as function of measuring temperature for LSCF and LNO-infiltrated LSCF cathodes, showing relative activation energies in the inset.
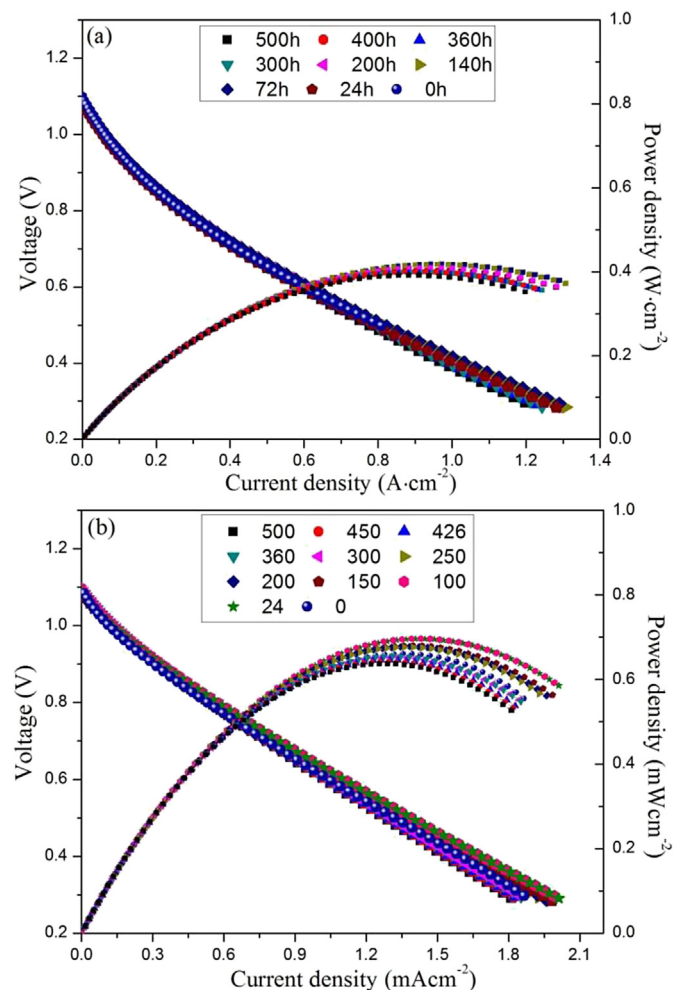

Fig. 5. Cell voltage and power density as function of current density for (a) pure LSCF and (b) LNO-infiltrated LSCF measured at 750 °C during cell operation of 500 h.

densities show an initial increase with the extension of time, indicating the activation process of cathode materials. The maximum power densities for the on cells with the cathodes of LSCF and LNO-infiltrated LSCF reach 418 and 697 mW cm^{-2} after a period of around 100 h, respectively. Hence, a 67% increase in the power density has been achieved through infiltration of LNO into LSCF backbone. Even after around 500 h, LNO-infiltrated LSCF still can deliver a power density of 637 mW cm^{-2}, which is much higher than pure LSCF electrode with power density of 392 mW cm^{-2} Fig. 6 indicates the voltage of the test cells as a function of time at a constant current density of 250 mA cm^{-2} at 750 °C. The obviously higher voltage achieved by using LNO-infiltrated LSCF, as compared to bare LSCF cathode, further confirms that the LNO nanoparticles can serve as a high-performance electrocatalyst. Both the baseline cell and the one with LNO coated LSCF cathode have experienced a degradation of voltage with the extension of time. In the case of bare LSCF cathode, the voltage drops from 0.841–0.839 to 0.839–0.836 V, showing a degradation rate of 0.36% over 500 h. This is lower than the values reported in the literatures (e.g. 0.9–1.5% per 1000 h) [29,30] for LSCF cathodes operated under similar conditions. The relatively high stability of bare LSCF cathode provides us a good baseline and high standard for the study of LNO infiltration.

In contrast, the cell using LNO-infiltrated LSCF cathode exhibits performance degradation of about 0.39% with a voltage drop from 0.952–0.949 to 0.949–0.946 V after 500 h. Thus, a slightly higher degradation rate is obtained for LNO-infiltrated LSCF cathode than LSCF itself. Compared to the reports of LSCF based cathodes including modified LSCF with other surface catalysts [6,31], which showed much higher degradation rates of the cathodes, the LNO-infiltrated LSCF cathodes with good long-term stability over 500 h seems to be a promising candidate for SOFC application. As far as the similar degradation rate for both LSCF and LNO-infiltrated LSCF cathodes is concerned, the extended durability measurements will be carried out in the future.

3.4. Discussion of degradation and ORR improvement

It has to be emphasized that the degradations observed for bare LSCF and LNO-infiltrated LSCF cathodes should be ascribed to different mechanisms. The performance loss with time for the bare LSCF could be associated with cation segregation, like the diffusion

Fig. 6. Cell voltage as function of time at a constant current density of 250 mA cm^{-2} for both bare LSCF and LNO-infiltrated LSCF.

of Sr and La into cathode surface, as widely suggested in the literatures [32–34]. While nanoparticle thermal coarsening or low-performance phase formation resulting from chemical instability [35–38] is usually responsible for long-term operation degradation of a cathode containing surface catalysts. In order to explain a relatively higher degradation rate of LNO-infiltrated LSCF cathode, the TEM and EDAX characterization analyses after the on-cell testing are depicted in Fig. 7. It can be observed that the growth of LNO nanoparticles from around 50 nm to 100–150 nm occurs after on-cell testing of 500 h. Correspondingly, the loss of surface area and 2PB/3PB active regions during the intermediate-temperature measurements could be responsible, at least in part, for the performance degradation the LNO-infiltrated LSCF cathode.

EDAX results of LNO-infiltrated LSCF cathode indicate that the diffusion of Sr, Fe and Co occurs from the LSCF to the LNO phase. The extraction of the cations from the LSCF perovskite lattice reveals the intrinsic instability of the LSCF cathode. As an acceptor, LNO materials could positively take advantage from the cation diffusion to enhance surface catalytic properties and ORR kinetics. The cobaltic electrode usually features fast oxygen surface exchange and high electrocatalytic activity for oxygen reduction. It has been reported that doped-Fe LNO, at least for small amount of Fe loading, have no influence on the electrocatalytic properties of LNO materials [39]. As to Sr doping into LNO, a possible reaction according to charge compensation may appear to increase the concentration of electron hole, as below,

$$2SrO + Ni_{Ni}^{\times} \leftrightarrow 2Sr'_{La} + Ni_{Ni}^{\cdot} + O_O^{\times}$$
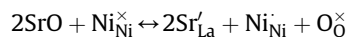
More importantly, a space charge layer at the LNO/LSCF heterostructured interface could be introduced based on charged transport and defect chemistry from the cation segregation. These facts might lead to the improved electrochemical performance and fast surface exchange of the LSCF based cathode. Certainly, evidence to support these hypotheses should be provided by evaluating the valence and amount of the Fe(IV)/Fe(III)/Fe(II), Co(IV)/Co(III)/Co(II), Ni(III)/Ni(II) and Sr (II) in the LNO infiltrant in the course of durability evolution. Further work on detailed characterizations associated with ORR process and kinetics of the composite cathodes will be thereby undertaken.

4. Concluding remarks

LNO nanoparticles have been successfully infiltrated into an LSCF backbone to obtain a new SOFC cathode for ORR kinetic consideration. The presented comparative study of LSCF and LNO-infiltrated LSCF shows a significant reduction in polarization resistance and a 67% increase in maximum power density by using LNO-infiltrated LSCF cathode. A power density of 637 mW cm^{-2} for the fuel cell using LNO-infiltrated LSCF cathode can still be achieved after long-term durability testing of about 500 h at 750 °C. The benefits from the presence of the LNO nanoparticles demonstrate that LNO-infiltrated LSCF materials can act as a highly active surface oxygen exchange cathode with promising electrochemical properties and fast ORR behavior. Although particle coarsening of LNO and cation diffusion from LSCF are observed, the preliminary stability measurements display a good long-term stability of the LNO-infiltrated LSCF cathode with a low OCV degradation rate of 0.39% over ~500 h at a constant current density of 250 mA cm^{-2}. It should be noted that the utilization of LNO infiltrant in the present work is different from that of being widely employed as surface electrocatalysts for alleviating Sr segregation issue of LSCF cathode. The cation segregation of LSCF could facilitate the surface catalytic properties and ORR kinetics of the LNO-infiltrated LSCF cathode with respect to favorable acceptance by LNO of Sr/Co doping.
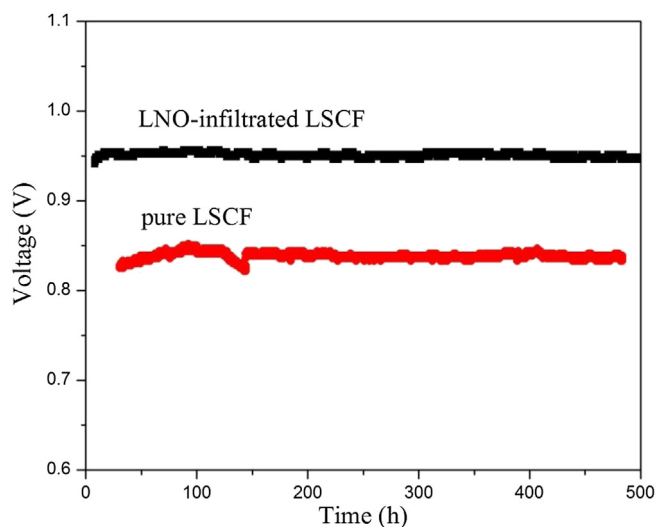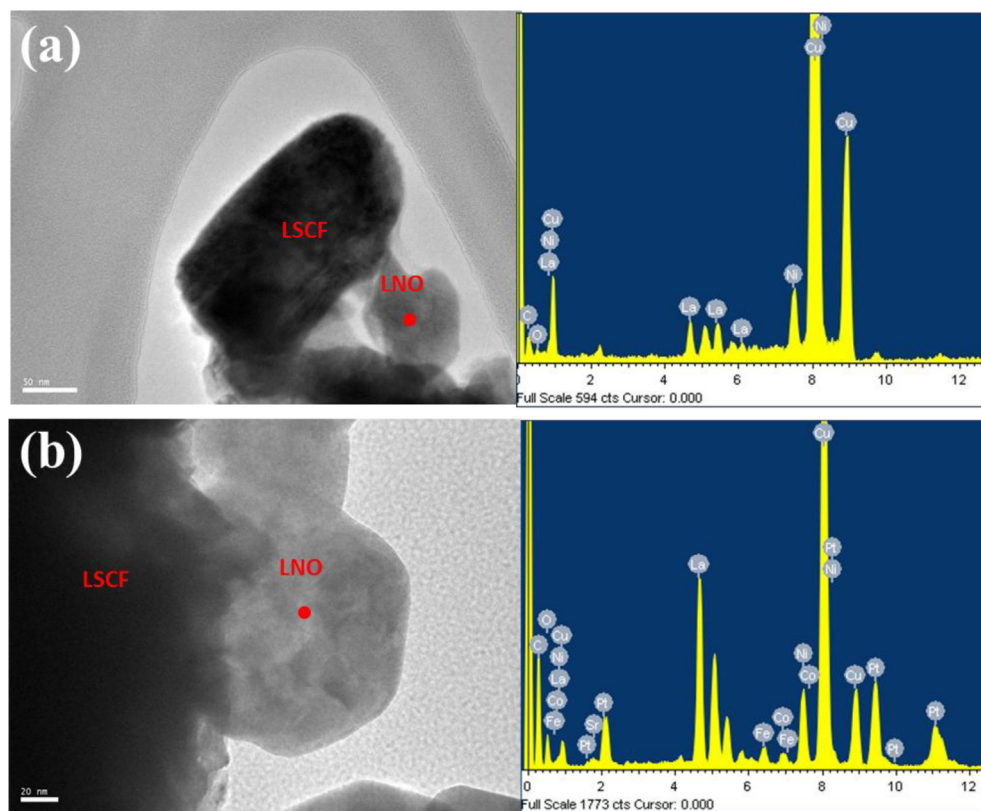
Fig. 7. TEM images and EDAXspectra of LNO-infiltrated LSCF cathode (a) before on-cell testing and (b) after long term testing.

However, in-depth details of enhanced surface oxygen exchange based on the use of LNO and intrinsic LNO/LSCF interaction should be investigated in the future.

References

[1] G. Kim, S. Wang, A. Jacobson, L. Reimus, P. Brodersen, C. Mims, J. Mater. Chem. 17 (2007) 2500–2505.
[2] L.-P. Sun, Q. Li, H. Zhao, L.-H. Huo, J.-C. Grenier, J. Power Sources 183 (2008) 43–48.
[3] Jiyoun Kim, Won-yong Seo, Jeeyoung Shin, Meilin Liu, Guntae Kim, J. Mater. Chem. A 1 (2013) 515–519.
[4] C. Setevich, F. Prado, D.Z. de Florio, A. Caneiro, J. Power Sources 247 (2014) 264–272.
[5] Y. Teraoka, H.M. Zhang, K. Okamoto, N. Yamazoe, Mater. Res. Bull. 23 (1) (1988) 51–58.
[6] S.B. Adler, Chem. Rev. 104 (10) (2004) 4791–4844.
[7] S.P. Jiang, Solid State Ionics 146 (1) (2002) 1–22.
[8] D. Oh, D. Gostovic, E.D. Wachsman, J. Mater. Res. 27 (15) (2012) 1992–1999.
[9] Y. Li, K. Gerdes, T. Horita, X. Liu, J. Electrochem. Soc. 160 (4) (2013) F343–F350.
[10] J. Chen, F. Liang, B. Chi, J. Pu, S.P. Jiang, J. Power Sources 194 (1) (2009) 275–280.
[11] L. Nie, M. Liu, Y. Zhang, M. Liu, J. Power Sources 195 (15) (2010) 4704–4708.
[12] M. Sahibzada, S.J. Benson, R.A. Rudkin, J.A. Kilner, Solid State Ionics 113 (1998) 285–290.
[13] S.J. Skinner, J.A. Kilner, Solid State Ionics 135 (1) (2000) 709–712.
[14] A. Tarancón, M. Burriel, J. Santiso, S.J. Skinner, J.A. Kilner, J. Mater. Chem. 20 (19) (2010) 3799–3813.
[15] V.L.E. Simonsen, L. Nørskov, A. Hagen, K.K. Hansen, J. Solid State Electrochem. 13 (10) (2009) 1529–1534.
[16] K. Kammer, Ionics 15 (3) (2009) 325–328.
[17] Yunhui Gong, Diego Palacio, Xueyan Song, Rajankumar L. Patel, Xinhua Liang, Xuan Zhao, John B. Goodenough, Kevin Huang, Nano Lett. 13 (2013) 4340–4345.
[18] Dong Ding, Mingfei Liu, Zhangbo Liu, Xiaxi Li, Kevin Blinn, Xingbao Zhu, Meilin Liu, Adv. Energy Mater. 3 (2013) 1149–1154.
[19] Mingfei Liu, Dong Ding, Kevin Blinn, Xiaxi Li, Lifang Nie, Meilin Liu, Int. J. Hydrogen Energy 37 (2012) 8613–8620.
[20] M.E. Lynch, L. Yang, W. Qin, J.-J. Choi, M. Liu, K. Blinn, M. Liu, Energy Environ. Sci. 4 (2011) 2249–2258.
[21] E.J. Crumlin, E. Mutoro, S.J. Ahn, G.J. la O', D.N. Leonard, A. Borisevich, Y. Shao-Horn, J. Phys. Chem. Lett. 1 (21) (2010) 3149–3155.
[22] E.J. Crumlin, S.J. Ahn, D. Lee, E. Mutoro, M.D. Biegalski, H.M. Christen, Y. Shao-Horn, J. Electrochem. Soc. 159 (7) (2012) F219–F225.
[23] J.B. Goodenough, S. Ramasesha, Mater. Res. Bull. 17 (3) (1982) 383–390.
[24] H. Zhao, L. Huo, L. Sun, L. Yu, S. Gao, J. Zhao, Mater. Chem. Phys. 88 (1) (2004) 160–166.
[25] K. Zhao, Q. Xu, D.P. Huang, M. Chen, B.H. Kim, Ionics 17 (3) (2011) 247–254.
[26] D. Chen, R. Ran, K. Zhang, J. Wang, Z. Shao, J. Power Sources 188 (1) (2009) 96–105.
[27] X. Lou, S. Wang, Z. Liu, L. Yang, M. Liu, Solid State Ionics 180 (23) (2009) 1285–1289.
[28] E. Perry Murray, M.J. Sever, S.A. Barnett, Solid State Ionics 148 (1) (2002) 27–34.
[29] F. Tietz, V.A.C. Haanappel, A. Mai, J. Mertens, D. Stöver, J. Power Sources 156 (1) (2006) 20–22.
[30] A. Mai, V.A. Haanappel, S. Uhlenbruck, F. Tietz, D. Stöver, Solid State Ionics 176 (15) (2005) 1341–1350.
[31] Steven P. Simner, Michael D. Anderson, James E. Coleman, Jeffry W. Stevenson, J. Power Sources 161 (2006) 115–122.
[32] F. Tietz, A. Mai, D. Stöver, Solid State Ionics 179 (2008) 1509–1515.
[33] S.P. Simner, M.D. Anderson, M.H. Engelhard, J.W. Stevenson, Electrochem. Solid-state Lett. 9 (2006) A478–A481.
[34] J.S. Hardy, J.W. Templeton, D.J. Edwards, Z.G. Lu, J.W. Stevenson, J. Power Sources 198 (2012) 76–82.
[35] Megna Shah, Peter W. Voorhees, Scott A. Barnett, Solid State Ionics 187 (2011) 64–67.
[36] San Ping Jiang, Int. J. Hydrogen 37 (2012) 449–470.
[37] Shiwoo Lee, Nicholas Miller, Kirk Gerdes, J. Electrochem. Soc. 159 (7) (2012) F301–F308.
[38] Dong Ding, Xiaxi Li, Samson Yuxiu Lai, Kirk Gerdes, Meilin Liu, Energy Environ. Sci. 7 (2014) 552–575.
[39] E. Boehm, J.M. Bassat, P. Dordor, F. Mauvy, J.C. Grenier, P. Stevens, Solid State Ion. 176 (37) (2005) 2717–2725.